AFM lithography and fabrication of multifunctional nanostructures with perovskite oxides

Run-Wei Li

Ningbo Institute of Materials Technology and Engineering (NIMTE),
Chinese Academy of Sciences (CAS),
Ningbo, Zhejiang 315201, PR China
E-mail: runweili@nimte.ac.cn

Abstract: Recent progress on atomic force microscopy (AFM) lithography on perovskite oxides, including doped $SrTiO_3$ single crystalline substrates and artificial perovskite manganite films, are reviewed systematically. $SrTiO_3$ is the commercial substrate extensively used for epitaxially growing perovskite oxide films and also a popular film material for fabricating functionalised devices. Perovskite manganite films are very promising candidate materials for spintronic devices and magnetic sensors. By combining AFM lithography and other techniques, such as film deposition, photo lithography, and wet etching etc., multifunctional nanodevices/nanostructures composed of perovskite oxides can be created.

Keywords: AFM; atomic force microscopy; nanolithography; nanostructure; nanodevice; perovskite oxide.

Reference to this paper should be made as follows: Li, R-W. (2009) 'AFM lithography and fabrication of multifunctional nanostructures with perovskite oxides', *Int. J. Nanotechnol.*, Vol. 6, No. 12, pp.1067–1085.

Biographical notes: Run-Wei Li is a Professor in Ningbo Institute of Materials Technology and Engineering (NIMTE), Chinese Academy of Sciences (CAS), China. He obtained his PhD in Condensed Matter Physics from Institute of Physics (IOP), CAS in 2002. Then he spent 13 months in Institute of Scientific and Industrial Research (ISIR), Osaka University, Japan as a JSPS (Japan Society for the Promotion of Science) fellow. From October 2003, he stayed in Germany as an Alexander von Humboldt fellow for 16 months. From February 2005, he worked in International Center for Young Scientists (ICYS), National Institute for Materials Sciences (NIMS), Japan as an ICYS research fellow for three years and two months. He joined in NIMTE as a Professor in 2007. His research focuses on multifunctional oxides and devices, magnetoelectronic/spintronic materials, physics and devices. He has published more than 50 peer-reviewed papers in international journals, such as *PNAS*, *Phys. Rev. B*, *Appl. Phys. Lett.*, *J. Appl. Phys.*, *Nanotechnology*, etc.

1 Introduction

In the past two decades, nanoscience and nanotechnology have been the worldwide hottest research fields [1,2]. Currently, more and more researchers are just attempting to generate and understand the functionalities of nanostructured materials and surfaces

based on well-controllable growth of nanomaterials and also so-called top-down lithography techniques, such as photo lithography, e-beam lithography, ion beam lithography, nano imprint, dip-pen, and scanning probe lithography etc. In the progress of constructing and understanding nanostructured materials and surfaces, scanning probe microscope (SPM) has played and also is playing very significant roles. Since Binnig and Rohrer invented scanning tunnelling microscope (STM) in 1981 [3], SPM families including atomic force microscope (AFM), magnetic force microscope (MFM), electrostatic force microscope (EFM) etc., have been used as powerful 'eyes' to reveal the microscopic world, and also used as 'hands' to control and manipulate the microscopic world. For example, by means of SPM, four processes can be used to construct nanostructures or fabricate nanostructured surfaces. As shown in Figure 1(a) atomic/molecule/cluster/particle manipulation [4–6]: electrostatic, chemical, or mechanical forces between the tip and samples allow a selective removal of individual atomic/molecule/cluster/particle from the surface and subsequent redeposition elsewhere with an atomic-level precision, which makes an SPM tip capable to manufacture nanostructures by direct manipulation of nanoparticles, clusters, molecules, or even single atoms; Figure 1(b) mechanical and thermomechanical patterning: an SPM probe tip can be used as a mechanical tool to create pits, lines, or craters in a soft resist layer. The resist patterns can then be transferred into the substrate through a direct etching or a lift-off process [7–9]; Figure 1(c) local electron exposure: the concentrated high electric field under a biased probe tip enables the field emission of electron from the tip. If a sample is coated with a thin resist, the emitted electrons can traverse the resist. The resist pattern can then be transferred into substrate by using a selective chemical etching or dry etching; and Figure 1(d) local oxidation (anodic oxidation) or chemical reaction: A voltage bias between a sharp tip and a sample generates an intense electric field in the vicinity of the tip. The intense electric field can ionise water molecules in the air or absorbed on the surface, and create negatively charged oxygen ions. These oxygen ions can react with the sample (usually for metal or semiconductor samples) to form an oxide film.

Figure 1 Four SPM-based processes available for nanolithography, (a) atomic/molecule/cluster/particle manipulation; (b) mechanical and thermomechanical patterning; (c) local electron exposure; and (d) local oxidation (anodic oxidation) or local chemical reaction (see online version for colours)

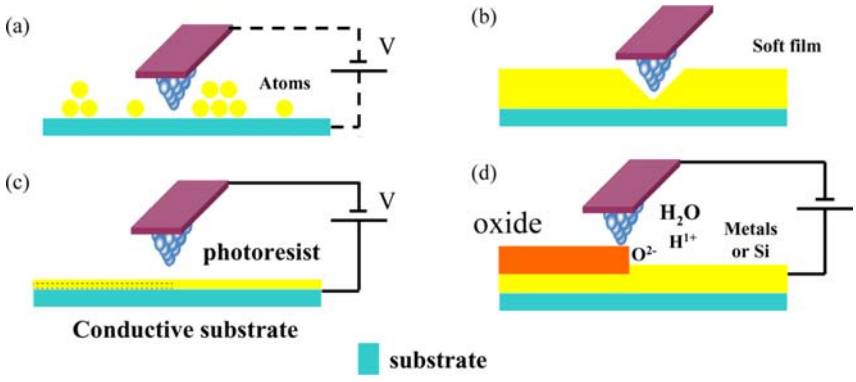

In 1990, Dagata et al. [10] oxidised hydrogen-passivated silicon surfaces using STM. The oxide feature can be used as an etching mask or an insulating barrier. Since then, this method based on the local oxidation or chemical reaction was named SPM lithography (sometimes anodic oxidation as well), which became a highly promising method for nanolithography and fabricating nanodevices. There are five advantages of SPM lithography.

1 *Maskless lithography*: No mask is needed for SPM lithography which makes this method especially suitable for self-assembled materials. As for the other lithography methods, a pre-designed mask is required. However, one is usually not able to control the growth of a self-assembled sample according to the pre-designed mask. By means of SPM lithography, we can perform nanolithography anywhere we want.

2 *Multi-functional*: As aforementioned, not only local oxidation or chemical reaction can be used, but also Figure 1(a) atomic/molecule/cluster/particle manipulation, Figure 1(b) mechanical and thermomechanical patterning, Figure 1(c) local electron exposure can be utilised to construct nanostructures in the same time based on the SPM tip.

3 *High resolution*: The best resolution of SPM lithography reported was about 10 nm [11].

4 *Detectable in real-time and in situ*: The topography of written patterns can be observed in situ after SPM lithography.

5 Chemical reactions driven by SPM tips, one can create new matters (oxides) on sample surfaces anywhere desired without any thermal process.

SPM lithography has been used for metals such as Ti [12], Cr [13], Nb [14], Al etc. [15–17], some semiconductors, including single crystalline and amorphous silicon [18–27]. Notably, SPM lithography has been gradually used in perovskite oxides, such as high-T_C superconductors [28–35], doped $SrTiO_3$ [36–38], perovskite manganites [39–43]. The mechanism of SPM lithography in oxides is more complicated, and can not be simply attributed to an electrochemical oxidation induced by intense electric field or current between the sample surface and the SPM tip as occurs on metal and semiconductor surfaces. Though the underlying physical process and mechanism of SPM lithography on oxides remain unclear, SPM lithography has become a very powerful tool for fabricating multifunctional nanostructures or devices and investigating the related mesoscopic physics especially in the strongly related electronic systems. As is well known, perovskite oxides have been dubbed an 'inorganic chameleon' and been considered as excellent candidate materials for fabricating multifunctional nanodevices due to their rich physical properties such as ferroelectricity, ferromagnetism (colossal magnetoresistive manganites), superconductivity, and semiconductivity. Undoubtedly, employing SPM lithography in perovskite oxides is very important especially for the realm of nanodevices.

In this review, we will focus on the progress on AFM lithography in

a perovskite oxides, including on $SrTiO_3$ single crystalline substrates which are the most widely used substrates for epitaxially growing perovskite oxide films

b perovskite manganite films which are promising candidate materials for sensor and spintronic devices.

2 Creation and control of AFM lithography patterns

2.1 AFM lithography on $SrTiO_3$ single crystalline substrates

$SrTiO_3$ is one type of very important insulating material for fabricating devices and also a popular single crystalline substrate widely used for epitaxially growing perovskite oxide films. In order to fabricate nanostructures with perovskite oxides, one approach is to prepare nanostructured substrates, then grow oxide films or nano-clusters/ nano-particles on the pre-patterned substrates. Therefore, the fabrication of nanostructured $SrTiO_3$ single crystalline substrates is very important for fabricating multifunctional nanodevices based on perovskite oxides.

AFM lithography can not be performed directly on $SrTiO_3$ single crystalline substrates because a voltage bias between the sample surface and the AFM tip is not able to be easily applied due to the high resistivity of $SrTiO_3$,. However, in the doped $SrTiO_3$ single crystals or films, for example, in Nb-doped $SrTiO_3$ (doping Nb at Ti-sites) single crystalline substrates or $SrTiO_{3-\delta}$ (oxygen vacancy doped) films, AFM lithography has been realised successfully. It is known that for AFM lithography processes in metals and semiconductors, a positive sample bias is necessary, and no pattern can be obtained under a negative sample bias. Similarly, for the doped $SrTiO_3$ substrates, nanopatterns can be written well by AFM lithography under a positive sample bias, but not under a negative sample bias.

Figure 2(a) shows, as an example, a topology of patterned Nb-$SrTiO_3$ (001) [$Sr(Ti_{0.99}Nb_{0.01})O_3$] surface. AFM (JEOL JSPM-4200) mounted with Pt-coated tip was used to perform AFM lithography on Nb-$SrTiO_3$ single crystalline substrates. A $5 \times 5 \times 0.5$ mm^3 Nb-$SrTiO_3$ substrate was fixed on a copper sample stage by a conductive paste. The AFM tip was grounded. The AFM lithography was performed by tapping mode. After the AFM lithography, topologies were observed by AFM *in situ* with a tapping mode. The height of the patterns on Nb-$SrTiO_3$(001) surface decreases with decreasing sample bias. Patterns with a width below 100 nm have been obtained. Under a negative sample bias, no patterns were obtained up to –10V. As shown in Figure 2(b), under the positive sample bias, there exists a threshold voltage (~2V), below which no patterns appear. When the sample bias is higher than +5V, the height tends to saturate. The saturation heights are dependent on the surface index, the patterns on (111) surface are higher than those on (001) surface fabricated under a same sample bias. In addition, the sizes of AFM lithography patterns are very sensitive to the external environment, such as humidity etc.

Figure 2 (a) AFM lithography patterns on single crystalline Nb-$SrTiO_3$ (001) substrate, the patterns were written under a sample bias of 5, 4, 3, 2V, respectively, as marked in the image and (b) sample bias dependence of the line height on Nb-$SrTiO_3$ (001) and (111) substrates (see online version for colours)

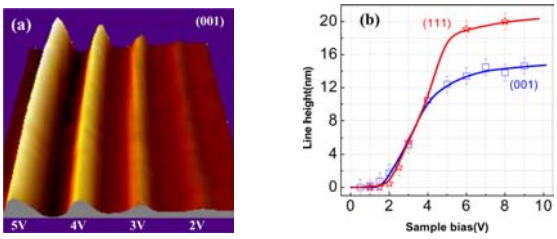

2.2 AFM lithography on perovskite manganite films

Perovskite manganites have attracted increasing interest over the last several years due to their fascinating physical properties, such as colossal magnetoresistance effects, metal-insulator transition, electron phase separation [44–51] and ~100% spin polarisation [52] etc. For example, lightly doped $La_{1-x}Ba_xMnO_3$ films exhibit room-temperature ferromagnetism even in an ultrathin film of 50Å. As a result, lightly doped $La_{1-x}Ba_xMnO_3$ film is considered as one of promising candidate materials for the realisation of room-temperature spintronic devices [53]. Undoubtedly, employing AFM lithography in perovskite manganite films is considerably important for both fabricating single nanosized spintronic devices and investigating the relevant mesoscopic physics in the strongly related electron systems.

We have investigated AFM lithography in perovskite manganite $La_{0.8}Ba_{0.2}MnO_3$ (LBMO) thin films with the aim to extend AFM lithography into perovskite manganites. It was found that controllable nano-sized patterns could be obtained with an excellent reproducibility under a negative sample bias rather than a positive one. This is completely different from doped $SrTiO_3$, where AFM lithography can be performed only under a positive sample bias, though $SrTiO_3$ and manganites are of a similar perovskite structure. The size of AFM lithography patterns could be well controlled by both the sample bias and the selection of tips.

LBMO films with a thickness 100 Å were deposited on $SrTiO_3$ (100) single crystal substrates by laser molecular beam epitaxy in an O_2 atmosphere with a pressure of 0.1 Pa. The substrate temperature was 730°C. The deposition rate was about 6.3 Å/min. All the fabricated films were annealed *in situ* with the growth conditions for 20 min and post annealed in 1 atm oxygen at 850°C for 10 h in order to avoid any oxygen deficiency. The film structure was confirmed by X-ray diffraction. All deposited films indicated atomically flat surfaces. Before AFM lithography, LBMO films were patterned into 10 μm-wide patterns by optical lithography and Ar-ion beam milling. AFM (JEOL JSPM-4200 and DI nanoman) mounted by conductive tips (Si cantilever coated by Pt, Cr-Co alloy, or W_2C) was used to perform AFM lithography with a contact mode in air. During AFM lithography, the tip scanning speed was 500 nm/s with the feedback on. After the AFM lithography and sequent wet etching, topologies were observed with tapping or contact modes.

At first, we performed AFM lithography on atomically flat LBMO surfaces under a positive sample bias as performed on doped $SrTiO_3$ substrates. Under completely same conditions, different surface structures appeared after AFM lithography processes, nano-gaps, trenches, mounds and grooves, and nanoparticles appeared alternately on LBMO films, as shown in Figure 3. Usually, the patterns were sub-micron-sized and lack of controllability and repeatability. It seemed very difficult to control the size and shape of the pattern though various positive sample biases were tried under various conditions.

However, when a negative sample bias was applied, nano-patterns were obtained with an excellent controllability and reproducibility. As a representative, Figure 4(a) shows the topography of a LBMO film patterned with a Pt-coated tip under various negative sample biases. The size of AFM lithography patterns could be well controlled by the sample bias and the selection of tips. Above a threshold voltage, the height of the pattern increased

with increasing sample bias linearly at first, then saturated at ~8, ~5, and ~4 nm for the tip coated by Pt, Cr-Co, and W_2C, respectively [as shown in Figure 4(c)]. The threshold voltage and saturation height were dependent on the type of the tip. The threshold voltage was about –4V for W_2C-coated tip, and about –3V for Pt-coated tip. The width of AFM lithography patterns also increased linearly with sample bias, and no saturation was observed up to a sample bias of –12V. Comparing Figure 4(c) and (d), one can find when the sample bias was above a saturation value, the increase of sample bias only made AFM lithography patterns increasing in width, but not in height. Compared to the sample bias and the selection of tips, reference voltage (which determines the distance or force between tip and sample surface) and tip scanning speed during AFM lithography were not important parameters for controlling the pattern height and width. The small line width and the interval in between two written lines of less than 50 nm by W_2C or Pt tip have been obtained.

Figure 3 Topography of $La_{0.8}Ba_{0.2}MnO_3$ films after AFM lithography under a positive sample bias of +8V. AFM lithography was uncontrollable under the positive sample biases (see online version for colours)

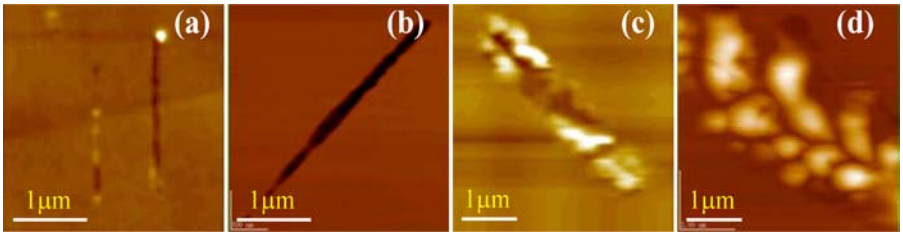

Figure 4 Topology of $La_{0.8}Ba_{0.2}MnO_3$ thin film patterned by AFM lithography with a Pt-coated tip under various negative sample biases (a); cross section (b); tip bias dependence of the height (c) and width (d) of AFM lithography patterns; tip bias is reversed to sample bias. Copyright 2005, IOP (see online version for colours)

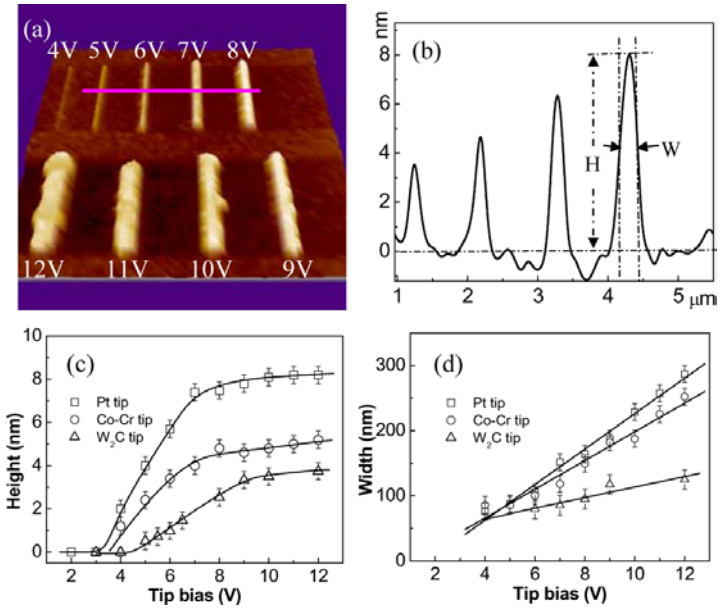

The sizes of AFM lithography patterns on LBMO films are dependent on the film quality. The height and width of patterns are larger on as-grown films than on annealed films in oxygen atmosphere. Moreover, when the film is very thin, the height of the AFM lithography pattern can be saturated even under a small sample bias.

3 Control of physical properties within nanoscale

By means of AFM lithography, we can fabricate nanopatterns, but also can manipulate the physical properties, such as mechanical, magnetic, electrical and even other physical properties within nanosized region anywhere desired.

Figure 5(a) and (b) show the AFM and FFM (friction force microscope) images of non-patterned LBMO surfaces. Terraced surfaces with the step height of one unit cell size (~0.4 nm) can be seen in Figure 5(a) and no obvious differences in FFM image. As shown in Figure 5(c), five lines were written, by contact mode, on LBMO film surface with a W_2C-coated tip under a sample bias of –8V. It can be clearly observed in Figure 5(d) that these AFM lithography patterns under a negative sample bias were of smaller friction forces compared to the non-patterned region. Because the normal loading force was kept constant during the whole observing process, one can conclude that the friction coefficient of the patterned region was smaller than that of non-patterned regions. In other words, by AFM lithography, we can make some region more lubricous even within tens nanometers.

Figure 5 AFM [(a) and (c)] and FFM [(b) and (d)] images of non-patterned $La_{0.8}Ba_{0.2}MnO_3$ film surfaces [(a) and (b)] and patterned with W_2C-coated tip under a sample bias of –8V [(c) and (d)]. Copyright 2005, IOP (see online version for colours)

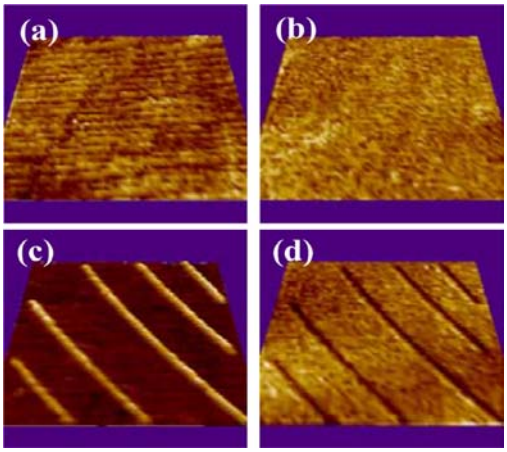

Figure 6(a) shows a planar double-gate field-effect transistor (FET) structure fabricated under a sample bias of –12V. The current-voltage (I-V) characteristics between electrode Source (S) and Drain (D), and between electrode S and Gate (G) were measured in the voltage range from –1 to +1V, respectively. As shown in Figure 6(b), under a voltage of 1V, the current was 1.7×10^{-6} A between electrode S and D, and 5.5×10^{-8} A

between electrode S and G, respectively. It is suggested that the patterned region was transformed into an insulating barrier, and the resistivity of the patterned region was 2 orders of magnitude higher than that of the non-patterned region.

Figure 6 (a) AFM image of an FET-like structure fabricated by AFM lithography under a sample bias of –12V on $La_{0.8}Ba_{0.2}MnO_3$ films patterned by optical lithography and ion beam shower and (b) I-V curves measured between S-D and S-G, the inset of Figure 6(b) is the amplified figure for S-G measurement (see online version for colours)

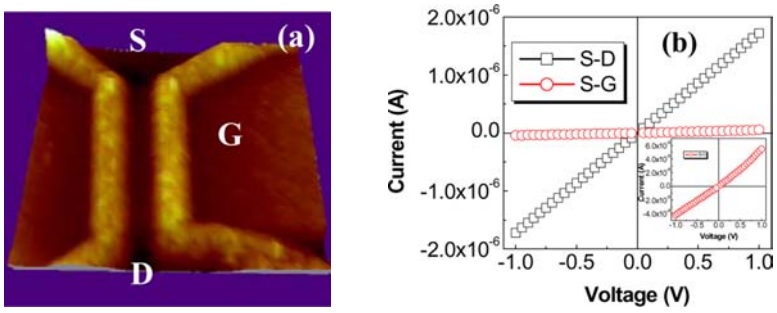

In addition, the ferromagnetism has been changed into paramagnetism within tens nanometre scale by AFM lithography in Fe_3O_4 thin films at room temperature [54]. It is also expected that the magnetism of the patterned region would also be modified by AFM lithography on the LBMO films as well based on the analogy of AFM lithography in Fe_3O_4 thin film.

4 High etching selection of the AFM lithography patterns

Though the nanolines fabricated by AFM lithography on LBMO films are more insulating compared to the non-patterned region, the resistivity of the patterned lines is still not high enough for fabricating FET structures. As shown in the inset of Figure 6(b), the leakage current is too big for an FET. Fortunately, the size-controllable patterns obtained under negative sample biases can be easily removed with a very high etching selectivity by a few seconds dip in diluted HCl solution, and be transformed into nano-sized grooves or vacuum gaps. As shown in Figure 7(a), two lines were written with Pt-coated tip under a sample bias of –10V and –8V, respectively, on LBMO film. The patterned sample was dipped in 10% HCl for 15 s. AFM lithography patterns were transferred into grooves [Figure 7(c)] with very sharp edges. The depth and width of such grooves were proportional to the height and width of the pre-existing lines [see Figure 7(b) and (d)]. In other words, the width and depth of grooves can be well controlled by the negative sample bias during AFM lithography. When the thickness of LBMO films is less then 20 nm, the etched nano-groove can penetrate the LBMO film and form a nanosized vacuum gap. Hirooka et al. [43] has achieved a LBMO nano-bridge with a width of less than 30 nm in between two vacuum gaps by combining AFM lithography and subsequent wet etching.

Figure 7 Topologies of patterned $La_{0.8}Ba_{0.2}MnO_3$ surface before (a) and after (c) wet etching. (b) and (d) show the cross sections of (a) and (c). Copyright 2004, AIP (see online version for colours)

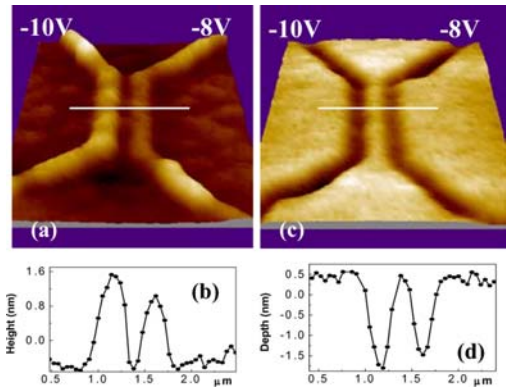

The resistance, as a function of temperature, of a LBMO channel with a 200 nm width [see Figure 8(b)] was measured by means of physical property measurement system (PPMS) under various magnetic fields. As shown in Figure 8(c) and (d), a metal-insulator transition appeared at ~320 K and a magnetoresistance peak appeared at ~300 K, which was basically consistent with that of non-patterned LBMO films [53]. In the low temperature range, a positive magnetoresistance appeared, which could be related to the domain wall effects of the sub-micro-sized channel. Therefore, except for the effects caused by the reduction of the channel size, AFM lithography and sequent wet etching did not destroy the physical properties of LBMO thin films, such as room-temperature ferromagnetism, metal-insulator transition, and colossal magnetoresistive effects. This point is very important for fabrication of nanodevices by combining AFM lithography and etching techniques.

Figure 8 Topologies of patterned $La_{0.8}Ba_{0.2}MnO_3$ surface (with Pt-coated tip under a sample bias of –10V) before (a) and after (b) wet etching. (c) and (d) show the resistance and magnetoresistance of the $La_{0.8}Ba_{0.2}MnO_3$ channel as a function of the temperature measured under various magnetic fields. The magnetoresistance (MR) was defined as MR = [R(H)–R(0)]/R(0) × 100%, where R(0) and R(H) are the resistance at absence and presence of a magnetic field. Copyright 2005, IOP (see online version for colours)

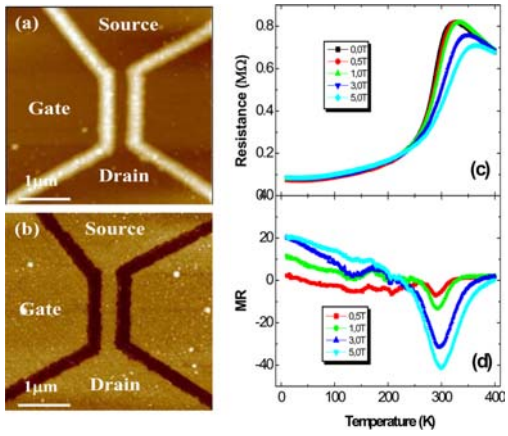

5 Relaxation behaviours of the AFM lithography patterns

Nanopatterns written by AFM lithography on perovskite oxide surfaces exhibit relaxation behaviours after patterning. For example, as shown in Figure 9(a), by tapping mode, three lines were written on the atomically flat $Sr(Ti,Nb)O_3$ (100) surface with a Pt-coated tip under a sample bias of +4V, +6V, and +8V, respectively (from left to right). The obtained lines by AFM lithography became smaller with time, and almost disappeared completely after 40 min except for several 'poles' remained. After enough long time (440 min), the entire surface relaxed to an atomically flat surface except for several 'poles' on some special spots [see Figure 9(d)]. Figure 9(e) and its inset show the time evolution of line height on $Sr(Ti,Nb)O_3$ (100) and (111) surfaces. Though there is an obvious difference between the initial line heights, the patterns on both $Sr(Ti,Nb)O_3$ (100) and (111) surfaces show basically consistent relaxation behaviours, the line height decreasing exponentially with time.

Figure 9 (a)–(d): Topography of patterned $Sr(Ti,Nb)O_3$ (100) surfaces as a function of time after patterning; the scanning scale is 5×5 μm; (e) Time dependence of line height on $Sr(Ti,Nb)O_3$ (100) and (111) surfaces, the inset shows the relationship between the line height and ln(time). Copyright 2004, AIP (see online version for colours)

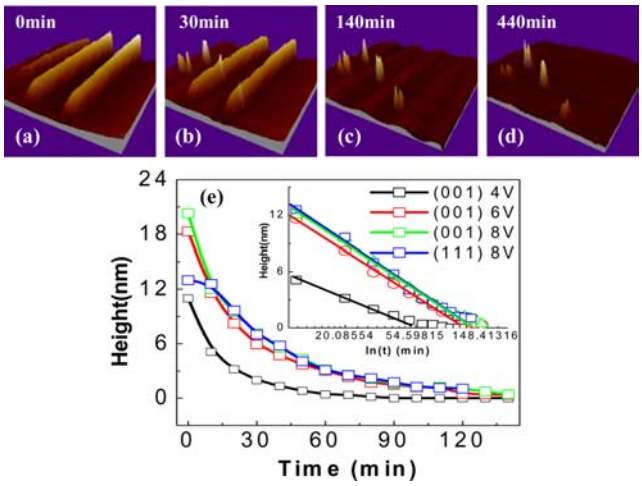

As shown in the inset of Figure 10, by contact mode, three lines were written on $Sr(Ti,Nb)O_3$ (100) surface with a W_2C-coated tip under a sample bias of +10V. I-V characteristics for the non-patterned and patterned regions (spot A and O in the inset of Figure 10) were measured by AFM mounted with W_2C-coated tip with a contact mode *in situ*. The current flowed through the substrate from up to down. As shown in Figure 10, the non-patterned region showed an insulative behaviour due to Schottky potential between the metal tip and the semiconductor sample. The patterned region is more insulating than the non-patterned one. For example, under a sample bias of +3V, the resistance of the patterned region ($\sim 10^{11}$ Ω) is three orders of magnitude larger than that of the non-patterned region ($\sim 10^{8}$ Ω). With elongating the time after patterning, the diffusion potential voltage, at which point the current started to increase dramatically, reduced, and the resistance of the patterned region decreases under a same voltage. Moreover, I-V curves approached gradually to that of the non-patterned region.

Consistent to the relaxation behaviours shown in Figure 9(a)–(d), the evolution of I-V characteristics also indicates the written patterns were not stable, and the height of the insulating pattern decreased with time.

Figure 10 The evolution of I-V characteristics of the patterned region on $Sr(Ti,Nb)O_3$ (100) surface (the spot O shown in the inset) with time; the orange dotted line shows the I-V characteristics of the non-patterned region (Spot A shown in the inset). Copyright 2004, AIP (see online version for colours)

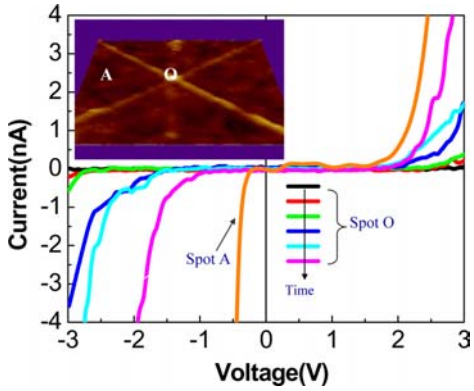

Similar to the observations in Nb-doped $SrTiO_3$ single crystal substrates, a slow relaxation behaviour of the AFM lithography patterns also appeared in the LBMO films. After laying the sample patterned by AFM lithography in air for a long time (for example 15 hours), the patterned lines became obscure, and the resistivity became smaller than measured immediately after AFM lithography [40].

The relaxation behaviour of the written patterns is obviously disadvantageous for constructing nano-devices by means of AFM lithography. Because the insulating materials created by AFM lithography can be used directly as a barrier, or be removed by wet etching to obtain a vacuum gap. The relaxation will limit the lifetime of the barrier or require a prompt wet etching after AFM lithography (within several minutes), which is a serious obstacle for applying this technique, especially in use of single crystal substrates due to the fast relaxation thereof. Fortunately, these remained 'poles' (as shown in Figure 9(a)–(d)) suggest the patterns were stable at some special places. It might be defects that stabilised the patterns. In order to verify this hypothesis, we bombarded the $Sr(Ti,Nb)O_3$ (100) surface by Ar ions with 100V accelerating voltage to create more surface defects. After that, AFM lithography was performed on the Ar-bombarded $Sr(Ti,Nb)O_3$ surface, and the stability of the created patterns was investigated. As shown in Figure 11(e)–(g), the patterns on the Ar-bombarded surface showed relaxation behaviour at first, and then stabilised with a height of several nanometers. What we should emphasise is, as shown in Figure 11(d), by comparing the 'poles' on the non-Ar-bombarded surface, the whole 'line' patterns on the Ar-bombarded surface showed very similar relaxation behaviours, even having an almost same final height (about 7 nm for that under the sample bias of +6V). Furthermore, much slower relaxation behaviours of nanopatterns created by AFM lithography were also observed in $SrTiO_{3-\delta}$ and LBMO films, in which more defects are expected

compared to the single crystal sample. These results also support that it was surface defects which depressed the relaxation and stabilised the written patterns.

Figure 11 Topography of patterned (a)–(c) $Sr(Ti,Nb)O_3$ (100) surface and (e-g): $Sr(Ti,Nb)O_3$ (100) surface bombarded by Ar ions as a function of time after patterning; the scanning scale is 5×5 μm; (d) Time dependence of the heights of 'line' patterns on Ar-bombarded $Sr(Ti,Nb)O_3$ (100) surface (blue solid line), comparing with that of 'line' patterns (black broken line) and 'pole' (red broken line) on non-Ar-bombarded $Sr(Ti,Nb)O_3$ (100) surface. Copyright 2004, AIP (see online version for colours)

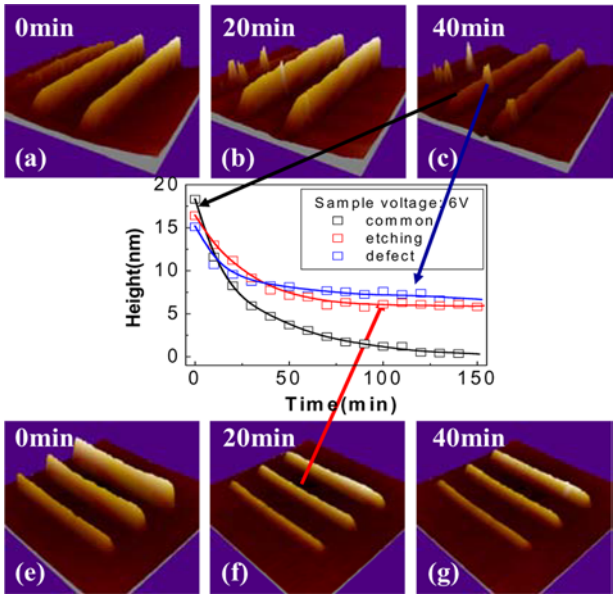

6 Possible mechanisms of AFM lithography in perovskite oxides

In metals and non-oxide semiconductors, the mechanism of AFM lithography has been supposed as an anodic oxidation induced by the intensive electric field in between AFM tip and the sample surface. It is proposed that AFM lithography causes an electrochemical reaction by scanning a biased probe close to the sample surface. Due to the ambient humidity in air, a water meniscus is formed between the probe and the sample surface. The intense electric field can ionise the water molecules on the surface, and create negatively charged oxygen ions. These oxygen ions can react with the sample (usually for metal or semiconductor samples) to form an oxide film. In order to assist this type of reaction, electrons should flow from tip to surface. Therefore, AFM lithography could be conducted only in positive sample biases over the threshold voltage on metal and Si surfaces.

As for AFM lithography in perovskite oxides, only anodic oxidation is obviously unable to be completely responsible for the underlying physical process. Compared to the oxygen-deficient $SrTiO_{3-\delta}$ films, oxygen vacancies are not very serious in

$Sr(Ti,Nb)O_3$ single crystalline substrates. However, AFM lithography can be well performed on $Sr(Ti,Nb)O_3$ single crystalline substrates. It seems that oxygen vacancies are not indispensable for AFM lithography in perovskite oxides. As a result, anodic oxidation should not the main physical process of AFM lithography in perovskite oxides. Except for the possible electrochemical oxidation of surface, chemical transport processes (for example, electromigration or field-induced diffusion [6,55]) might occur due to the intensive electric field in between the AFM tip and sample surface, which can explain the large volume expansion and the observed relaxation behaviours of the patterned region. The considerable relaxation of the patterns can be attributed to recovering from a poorly dense $SrTiO_3$ to initial state via chemical transport within nanoscale. Defects at surface prevent ion migration so that lines formed by AFM lithography remain steadily on the Ar-bombarded surface and 'poles' remain at the defect sites on untreated single crystal surfaces, respectively.

The polarisation dependence (positive or negative sample biases) of AFM lithography seems not to be related to the type of carrier. In p-doped WSe_2 [56], which is the same type of carrier (holes as carriers) as LBMO, AFM lithography patterns can be obtained only under a positive sample bias, however, the surface of WSe_2 was severely destroyed under a negative sample bias. Similar to the explanation for the AFM lithography in WSe_2, AFM lithography process under a positive sample bias on LBMO surfaces can be understood well based on field-induced electrochemical reaction and direct mechanical tip-sample abrasion. The FFM images indicated that different matters were created under different sample biases. Under a positive sample bias, field-induced electrochemical reaction created large patterns which indicated a larger friction force coefficient, part of the newly created patterns was removed by sequent mechanical abrasion. Under a negative sample bias, field-induced electrochemical reaction seems to more ambient. The newly created patterns were of a smaller friction force coefficient [see Figure (5)]. No significant mechanical abrasion occurred, as a result, controllable and reproducible patterns were obtained.

Based on the analysis aforementioned, the underlying physical process of the AFM lithography in perovskite oxides should be very complicated, probably not only one, but also several physical processes were involved, including electrochemical reaction, chemical transportation (such as electromigration or field-induced diffusion), and mechanical abrasion etc. Of course, in order to work out the exact mechanisms, more efforts are needed.

7 Applications of AFM lithography in perovskite oxides

Though the underlying physical mechanism of AFM lithography in oxide materials remains unclear so far, AFM lithography has been considered as a very powerful technique for fabricating nanostructures of functional oxides. Followings are some typical examples.

Pellegrino et al. [36] applied AFM lithography to semiconducting oxygen deficient $SrTiO_{3-\delta}$ thin films grown on $LaAlO_3$ substrates. In comparison with the as-grown film, the patterned regions present different electrical and structural properties, which can be exploited to realise submicrometer circuits. A prototype of a $SrTiO_{3-\delta}$-based side gate

FET was fabricated by AFM lithography and subsequent wet etching. The FET showed a 4% modulation of the channel resistivity with a gate voltage of 40V.

Yanagisawa et al. [42] applied AFM lithography in phase-separated manganite (La,Pr,Ca)MnO_3 films and fabricated manganite channel with various width. They examined the magnetoresistance behaviours of channel structures with different channel widths. The 500 nm channel showed an extremely sharp transition from a charge ordered insulator to a ferromagnetic metal at low temperature and some resistivity steps appeared with increasing magnetic field. Such extremely sharp insulator-metal transition can be understood based on that the channel width approaches the size of charge ordered cluster and the melting of one charge-ordered cluster under the applied magnetic field created a jump in the resistivity.

Kim et al. [57] employed AFM lithography and hydrothermal epitaxy processes to resolve issues related to aligning ferroelectric micro- and nano-sized cell arrays through a bottom-up approach. Nb-doped $SrTiO_3$ (100) surface was transformed in two dimensions by applying bias using a conductive AFM tip. The locally transformed areas were etched out with an acidic solution. It was found that the $PbTiO_3$ crystal nucleated and grew on the artificially aligned grooves preferentially during a hydrothermal epitaxial process. The self-patterned $PbTiO_3$ cell had excellent piezoresponse hysteresis with ferroelectric properties suitable for the fabrication of micro- and nano-sized ferroelectric devices.

In general, besides metals, Si, doped $SrTiO_3$ films and single crystals, perovskite manganite films, AFM lithography have been used in Fe_3O_4 and high-T_C superconductors. It is expected that the technique should be available for other functional oxide materials if only the resistance is relatively low that the voltage bias can be applied in between the sample surface and AFM tips. In other words, more application margin remains so far.

8 Fabrication of nanostructures by combining AFM lithography and other etching techniques

Figure 12 shows, as an example, a process for fabricating a planar double-gate FET structure on LBMO films by combining AFM lithography, optical lithography, wet etching and so on. First, (a) atomically flat LBMO films were grown on $SrTiO_3$ (100) single crystalline substrates by pulsed laser deposition (PLD) or laser-MBE systems [53,58]; (b) metal electrodes were deposited on the LBMO film by sputtering with a metal mask; (c–d) LBMO films were patterned into crossed patterns with a width of 10 μm in the desired region by optical lithography and Ar-ion beam milling. (e) AFM lithography performed on the remained LBMO films by means of AFM (JEOL JSPM-4200 or DI nanoman) mounted by conductive tips; (f) after AFM lithography, a rapid wet etching by diluted HCl solution to transform AFM lithography patterns into nanosized vacuum gaps. By means of such a process, some functional nanostructures could be fabricated simply, however, with a very high resolution.

Figure 12 AFM lithography procedure for fabricating nanostructures/nanodevices on perovskite oxides. (a) growth of manganite films by pulsed laser deposition (PLD), (b) deposition of metal electrodes by sputtering with a mask; (c) and (d) optical lithography and ion beam shower to remove the surplus manganite films; (e) AFM lithography on the remained manganite films and (f) wet etching to transform the AFM lithography patterns into nanogaps (see online version for colours)

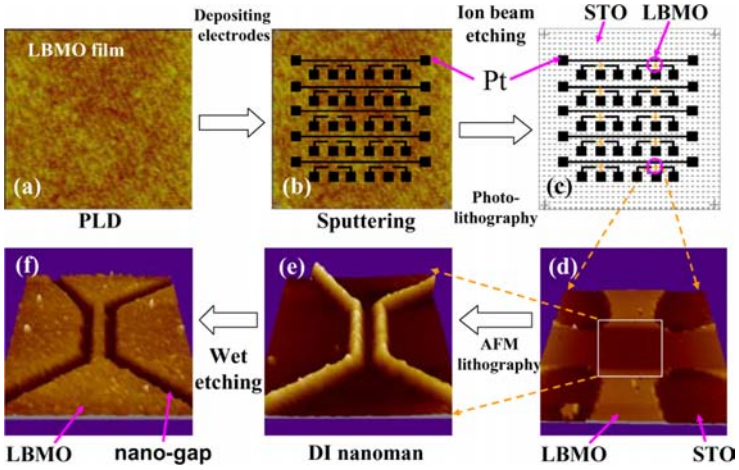

9 Conclusion and outlook

By means of AFM lithography, nano-patterns with a resolution of tens of nanometres and an excellent controllability and reproducibility have been realised in multifunctional perovskite oxides, including the doped $SrTiO_3$ single crystalline substrates, which are widely used for growing perovskite oxide films, and perovskite manganite films, which are very promising candidate materials for spintronic devices. The fabricated patterns indicate obvious relaxation behaviours. Introducing defects, for example, Ar-ion irradiations, was found to be a very effective strategy to make AFM lithography patterns stable. The physical properties, such as mechanical, electrical, and magnetic properties, can be modulated well within a nano-sized region by means of AFM lithography. AFM lithography patterns are of very high etching selectivity, and can be transformed into nano-sized vacuum gaps simply by a rapid wet etching. Importantly, AFM lithography and sequent wet etching do not destroy the important physical properties, such as room-temperature ferromagnetism, colossal magnetoresistive effects, and metal-insulator transition etc., of the perovskite oxides. It is expected that various multifunctional nanodevices, such as spin-field effect transistor [59] and the ferromagnetic single electron transistor, will be fabricated with the multifunctional perovskite oxides by combining optical lithography, AFM lithography, wet etching etc.

Due to the feature of AFM, currently, AFM lithography is not of a high output. However, with the development of multi-tip AFM [60,61] and high-speed AFM [62,63], the low output will be overcome. In addition, AFM lithography is performed usually in air and is very sensitive to the external environment, such as humidity. Pellegrino et al. [38] improved AFM lithography by controlling electrical current between the sample surfaces and the AFM tip instead of controlling the sample bias and realised AFM lithography that is much less sensitive to the external environment.

Acknowledgements

The author thanks Professor T. Kawai, Professor H. Tanaka, Dr. T. Kanki, Mr. M. Hirooka for their contributions to this work.

References

1 Moriarty, P. (2001) 'Nanostructured materials', *Rep. Prog. Phys.*, Vol. 64, pp.297–381.

2 Rosei, F. (2004) 'Nanostructured surfaces: challenges and frontiers in nanotechnology', *J. Phys.: Condens. Matter*, Vol. 16, pp.S1373–S1436.

3 Binnig, G. and Rohrer, H. (1982) 'Scanning tunneling microscopy', *Helv. Phys. Acta*, Vol. 55, pp.726–735.

4 Fishlock, T.W., Oral, A., Egdell, R.G. and Pethica, J.B. (2000) 'Manipulation of atoms across a surface at room temperature', *Nature*, Vol. 404, pp.743–745.

5 Baur, C., Bugacov, A., Koel, B.E., Madhukar, A., Montoya, N., Ramachandran, T.R., Requicha, A.A.G., Resch, R. and Will, P. (1998) 'Nanoparticle manipulation by mechanical pushing: underlying phenomena and real-time monitoring', *Nanotechnology*, Vol. 9, pp.360–364.

6 Stroscio, J.A. and Eigler, D.M. (1991) 'Atomic and molecular manipulation with the scanning tunneling microscope', *Science*, Vol. 254, pp.1319–1326.

7 Szoszkiewicz, R., Okada, T., Jones, S.C., Li, T-D., King, W.P., Marder, S.R. and Riedo, E. (2007) 'High-speed, sub-15 nm feature size thermochemical nanolithography', *Nano Lett.*, Vol. 7, pp.1064–1067.

8 Bouchiat, V. and Esteve, D. (1996) 'Lift-off lithography using an atomic force microscope', *Appl. Phys. Lett.*, Vol. 69, pp.3098–3100.

9 Sohn, L.L. and Willett, R.L. (1995) 'Fabrication of nanostructures using atomic-force-microscope-based lithography', *Appl. Phys. Lett*., Vol. 67, pp.1552–1554.

10 Dagata, J.A., Schneir, J., Harary, H.H., Evans, C.J., Postek, M.T. and Bennett, J. (1990) 'Modification of hydrogen-passivated silicon by a scanning tunneling microscope operating in air', *Appl. Phys. Lett*., Vol. 56, pp.2001–2003.

11 Snow, E.S. and Campbell, P.M. (1995) 'AFM fabrication of sub-10-nanometer metal-oxide devices with in situ control of electrical properties', *Science*, Vol. 270, pp.1639–1641.

12 Matsumoto, K., Ishii, M., Segawa, K., Oka, Y., Vartanian, B.J. and Harris, J.S. (1996) 'Room temperature operation of a single electron transistor made by the scanning tunneling microscope nanooxidation process for the TiO_x/Ti system', *Appl. Phys. Lett*., Vol. 68, pp.34–36.

13 Wang, D., Tsau, L. and Wang, K.L. (1995) 'Nanofabrication of thin chromium film deposited on Si(100) surfaces by tip induced anodization in atomic force microscopy', *Appl. Phys. Lett.*, Vol. 67, pp.1295–1297.

14 Delacour, C., Claudon, J., Poizat, J-Ph., Pannetier, B., Bouchiat, V., Villegier, J.C., Tarkhov, M., Korneev, A., Voronov, B. and Gol'tsman, G. (2007) 'Superconducting single photon detectors made by local oxidation with an atomic force microscope', *Appl. Phys. Lett.*, Vol. 90, pp.191116.

15 Irmer, B., Kehrie, M., Lorenz, H. and Kotthaus, J.P. (1997) 'Fabrication of Ti/TiO_x tunneling barriers by tapping mode atomic force microscopy induced local oxidation', *Appl. Phys. Lett.*, Vol.71, pp.1733–1735.

16 Snow, E.S., Park, D. and Campbell, P.M. (1996) 'Single-atom point contact devices fabricated with an atomic force microscope', *Appl. Phys. Lett*., Vol. 69, pp.269–271.

17 Snow, E.S., Campbell, P.M., Rendell, R.W., Buot, F.A., Park, D., Marrian, C.R.K. and Magno, R. (2002) 'A metal/oxide tunneling transistor', *Appl. Phys. Lett*., Vol. 72, pp.3071–3073.

18 Snow, E.S., Campbell, P.M. and McMarr, P.J. (1993) 'Fabrication of silicon nanostructures with a scanning tunneling microscope', *Appl. Phys. Lett.*, Vol. 63, pp.749–751.

19 Teuschier, T., Mahr, K., Miyazaki, S., Hundhausen, M. and Ley, L. (1995) 'Nanometer-scale field-induced oxidation of Si(111):H by a conducting-probe scanning force microscope: doping dependence and kinetics', *Appl. Phys. Lett*., Vol. 67, pp.3144–3146.

20 Avouris, P., Hertel, T. and Martel, R. (1997) 'Atomic force microscope tip-induced local oxidation of silicon: kinetics, mechanism, and nanofabrication', *Appl. Phys. Lett*., Vol. 71, pp.285–287.

21 Held, R., Vancura, T., Heinzel, T., Ensslin, K., Holl, M. and Wegscheider, W. (1998) 'In-plane gates and nanostructures fabricated by direct oxidation of semiconductor heterostructures with an atomic force microscope', *Appl. Phys. Lett*., Vol. 73, pp.262–264.

22 Garcia, R., Calleja, M. and Perez-Murano, F. (1998) 'Local oxidation of silicon surfaces by dynamic force microscopy: nanofabrication and water bridge formation', *Appl. Phys. Lett.*, Vol. 72, pp.2295–2297.

23 Legr, B. and Stievenard, D. (1999) 'Nanooxidation of silicon with an atomic force microscope: a pulsed voltage technique', *Appl. Phys. Lett*., Vol. 74, pp.4049–4051.

24 Tello, M. and Garcia, R. (2001) 'Nano-oxidation of silicon surfaces: comparison of noncontact and contact atomic-force microscopy methods', *Appl. Phys. Lett*., Vol. 79, pp.424–426.

25 Yang, M.J., Cheng, K.A., Yang, C.H. and Culbertson, J.C. (2002) 'A nanofabrication scheme for InAs/AlSb heterostructures', *Appl. Phys. Lett*., Vol. 80, pp.1201–1203.

26 Bo, X.Z., Rokhinson, L.P., Yin, H.Z., Tsui, D.C. and Sturm, J.C. (2002) 'Nanopatterning of Si/SiGe electrical devices by atomic force microscopy oxidation', *Appl. Phys. Lett.*, Vol. 81, pp.3263–3265.

27 Hwang, J.S., Hu, Z.S., You, Z.Y., Lin, T.Y., Hsiao, C.L. and Tu, L.W. (2006) 'Local oxidation of InN and GaN using an atomic force microscope', *Nanotechnology*, Vol. 17, pp.859–863.

28 Thomson, R.E., Morel, J. and Roshko, A. (1994) 'Surface modification of $YBa_2Cu_3O_{7\text{-delta}}$ thin films using the scanning tunneling microscope: five methods', *Nanotechnology*, Vol. 5, pp.57–69.

29 Heyvaert, I., Osquiguil, E., Van Haesendonck, C. and Bruynseraede, Y. (1992) 'Etching of screw dislocations in $YBa_2Cu_3O_7$ films with a scanning tunneling microscope', *Appl. Phys. Lett.*, Vol. 61, pp.111–113.

30 Bertsche, G., Clauss, W. and Kem, D.P. (1996) 'Nanometer-scale surface modifications of $YBa_2Cu_3O_{7-\delta}$ thin films using a scanning tunneling microscope', *Appl. Phys. Lett*., Vol. 68, pp.3632–3634.

31 Heinzelmann, H., Anselmetti, D., Wiesendanger, R., Güntherodt, H.J., Kaldis, E. and Wisard, A. (1988) 'Topography and local modification of the $HoBa_2Cu_3O_{7-x}$(001) surface using scanning tunneling microscopy', *Appl. Phys. Lett*., Vol. 53, pp.2447–2449.

32 Terashima, K., Kondoh, M., Takamura, Y., Komaki, H. and Yoshida, T. (1991) 'Surface modification of Bi-Sr-Ca-Cu-O films deposited *in situ* by radio frequency plasma flash evaporation with a scanning tunneling microscope', *Appl. Phys. Lett.*, Vol. 59, pp.644–646.

33 Parks, D.C., Wang, J., Clark, N.A. and Hermann, A.M. (1991) 'Scanning tunneling microscope surface imaging and etching of single crystals of the high-temperature superconductor $Tl_2Ba_2CuO_{6+\delta}$', *Appl. Phys. Lett.*, Vol. 59, pp.1506–1508.

34 Song, I., Kim, B.M. and Park, G. (1997) 'Fabrication of a Josephson junction using an atomic force microscope', *Appl. Phys. Lett.*, Vol. 76, pp.601–603.

35 Boneberg, J., Böhmisch, M., Ochmann, M. and Leiderer, P. (1997) 'Scanning probe nanostructuring of $YBa_2Cu_3O_7$: a corrosion induced abrasion', *Appl. Phys. Lett.*, Vol. 71, pp.3805–3807.

36 Pellegrino, L., Pallecchi, I., Marré, D., Bellingeri, E. and Siri, A.S. (2002) 'Fabrication of submicron-scale $SrTiO_{3-\delta}$ devices by an atomic force microscope', *Appl. Phys. Lett*., Vol. 81, pp.3849–3851.

37 Li, R.W., Kanki, T., Tanaka, H., Takagi, A., Matsumoto, T. and Kawai, T. (2004) 'Relaxation of nanopatterns on Nb-doped $SrTiO_3$ surface', *Appl. Phys. Lett*., Vol. 84, pp.2670–2672.

38 Pellegrino, L., Bellingeri, E., Siri, A.S. and Marré, D. (2005) 'Current-controlled lithography on conducting $SrTiO_{3-\delta}$ thin films by atomic force microscopy', *Appl. Phys. Lett*., Vol. 87, pp.064102.

39 Li, R.W., Kanki, T., Tohyama, H.A., Zhang, J., Tanaka, H., Takagi, A., Matsumoto, T. and Kawai, S.T. (2004) 'Atomic force microscope lithography in perovskite manganite $La_{0.8}Ba_{0.2}MnO_3$ films', *J. Appl. Phys.*, Vol. 95, pp.7091–7093.

40 Li, R.W., Kanki, T., Tohyama, H.A., Hirooka, M., Tanaka, H. and Kawai, T. (2005) 'Nanopatterning of perovskite manganite thin films by atomic force microscope lithography', *Nanotechnology*, Vol. 16, pp.28–31.

41 Yanagisawa, Y., Hirooka, M., Tanaka, H., Kawai, T. (2006) 'Nanoscale patterning of $(La,Pr,Ca)MnO_3$ thin film using atomic force microscopy lithography and their electrical properties', *J. Appl. Phys.*, Vol. 100, pp.124316.

42 Yanagisawa, Y., Tanaka, H., Kawai, T. and Pellegrino, L. (2006) 'Digitalized magnetoresistance observed in $(La,Pr,Ca)MnO_3$ nanochannel structures', *Appl. Phys. Lett.*, Vol. 89, pp.253121.

43 Hirooka, M., Yanagisawa, Y., Kanki, T., Tanaka, H. and Kawai, T. (2006) 'Fabrication of sub-50 nm $(La,Ba)MnO_3$ ferromagnetic nanochannels by atomic force microscopy lithography and their electrical properties', *Appl. Phys. Lett*., Vol. 89, pp.163113.

44 Tokura, Y. and Tomioka, Y. (1999) 'Colossal magnetoresistive manganites', *J. Magn. Magn. Mater.*, Vol. 200, pp.1–23.

45 Dagotto, E., Hotta, T. and Moreo, A. (2001) 'Colossal magnetoresistant materials: the key role of phase separation', *Phys. Rep.*, Vol. 344, pp.1–153.

46 Li, R.W., Sun, J.R., Li, Q.A., Zhu, T., Zhang, S.Y. and Shen, B.G. (2003) 'Magnetic transition and large low-field magnetoresistance near Curie temperature in polycrystalline $La_{2/3}A_{1/3}MnO_3$ (A = Ca, Sr)', *J. Appl. Phys*., Vol. 93, pp.8092–8094.

47 Li, R.W., Wang, Z.H., Wang, W.N., Sun, J.R., Li, Q.A., Zhang, S.Y., Cheng, Z.H., Shen, B.G. and Gu, B.X. (2002) 'Large low-field magnetoresistance of phase-separated single crystalline $Pr_{0.7}Pb_{0.3}MnO_3$', *Appl. Phys. Lett*., Vol. 80, pp.3367–3369.

48 Li, R.W., Zhou, X., Belik, A., Inoue, J., Miki, K. and Shen, B.G. (2006) 'Current effects and topology of metallic phase in single crystalline $Pr_{0.7}Pb_{0.3}MnO_3$', *J. Appl. Phys*., Vol. 100, pp.113902.

49 Li, R.W., Zhou, X., Shen, B.G. and Hillebrands, B. (2005) 'Process dependence of transport properties in phase-separated $Pr_{0.7}Pb_{0.3}MnO_3$ single crystal', *Phys. Rev. B*, Vol. 71, pp.092407.

50 Li, R.W., Sun, J.R., Li, Q.A., Wang, Z.H., Zhang, S.Y., Cheng, Z.H., Zhao, H.W. and Shen, B.G. (2002) 'Phase separation induced by doping at Mn-sites in $Nd_{0.5}Ca_{0.5}Mn_{0.98}Ga_{0.02}O_3$', *J. Appl. Phys*., Vol. 91, pp.7941–7943.

51 Li, R.W., Zhang, Z.R., Li, Q.A., Sun, J.R., Wang, G.J., Cheng, Z.H., Wang, Z.H., Zhang, S.Y., Han, B.S. and Shen, B.G. (2002) 'Direct observation of phase separation in $La_{0.45}Sr_{0.55}MnO_{3-\delta}$ ($\delta \approx 0.01$)', *J. Appl. Phys*., Vol. 92, pp.7404–7407.

52 Dörr, K. (2006) 'Ferromagnetic manganites: spin-polarized conduction versus competing interactions', *J. Phys. D: Appl. Phys.*, Vol. 39, pp.R125–R150.

53 Kanki, T., Li, R.W., Naitoh, Y., Tanaka, H., Matsumoto, T. and Kawai, T. (2003) 'Nanoscale observation of room-temperature ferromagnetism on ultrathin $(La,Ba)MnO_3$ films', *Appl. Phys. Lett*., Vol. 83, pp.1184–1186.

54 Hirooka, M., Tanaka, H., Li, R.W. and Kawai, T. (2004) 'Nanoscale modification of electrical and magnetic properties of Fe_3O_4 thin film by atomic force microscopy lithography', *Appl. Phys. Lett*., Vol. 85, pp.1811–1813.

55 Kondo, S., Heike, S., Lutwyche, M. and Wada, Y. (1995) 'Surface modification mechanism of materials with scanning tunneling microscope', *J. Appl. Phys*., Vol. 78, pp.155–160.

56 Böhmisch, M., Burmeister, F., Boneberg, J. and Leiderer, P. (1996) 'Nanostructuring on WSe_2 with the atomic force microscope by a potential controlled electrochemical reaction', *Appl. Phys. Lett*., Vol. 69, pp.1882–1884.

57 Kim, R.H., Ahn, H.W., Han, S.H. and Choi, S.K. (2007) 'Two-dimensional self-patterning of $PbTiO_3$ on a Nb–$SrTiO_3$ (001) surface using atomic force microscope lithography and hydrothermal epitaxy', *Appl. Phys. Lett.*, Vol. 90, pp.172907.

58 Li, R.W., Kanki, T., Tohyama, H.A., Zhang, J., Tanaka, H. and Kawai, T. (2004) 'Ordered nano-islands on (La,Ba)MnO_3 thin film surface by self-organization', *J. Nanosci. Nanotechnol.*, Vol. 4, pp.982–985.

59 Ahn, C.H., Triscone, J-M. and Mannhart, J. (2003) 'Electric field effect in correlated oxide systems', *Nature*, Vol. 424, pp.1015–1018.

60 Minne, S.C., Yaralioglu, G., Manalis, S.R., Adams, J.D., Zesch, J., Atalar, A. and Quate, C.F. (1998) 'Automated parallel high-speed atomic force microscopy', *Appl. Phys. Lett*., Vol. 72, pp.2340–2342.

61 Minne, S.C., Adams, J.D., Yaralioglu, G., Manalis, S.R., Atalar, A. and Quate, C.F. (1998) 'Centimeter scale atomic force microscope imaging and lithography', *Appl. Phys. Lett.*, Vol. 73, pp.1742–1744.

62 Schitter, G., Allgöwer, F. and Stemmer, A. (2004) 'A new control strategy for high-speed atomic force microscopy', *Nanotechnology*, Vol. 15, pp.108–114.

63 Humphris, A.D.L., Miles, M.J. and Hobbs, J.K. (2005) 'A mechanical microscope: high-speed atomic force microscopy', *Appl. Phys. Lett.*, Vol. 86, pp.034106.